AGN

METEOROID IMPACT SIMULATION

by

MAGNETIC GRADIENT PARTICLE ACCELERATION TECHNIQUES

Contract NAS 8-11174

George C. Marshall Space Flight Center
National Aeronautics and Space Administration
Huntsville, Alabama

AN-1460

Quarterly Progress Report
1 July 1965 through 30 September 1965

AN-1460

METEOROID IMPACT SIMULATION

by

MAGNETIC GRADIENT PARTICLE ACCELERATION TECHNIQUES

Contract NAS 8-11174

George C. Marshall Space Flight Center
National Aeronautics and Space Administration
Huntsville, Alabama

Quarterly Progress Report

1 July 1965 through 30 September 1965

Robert L. Chapman
Principal Investigator
Aerojet-General Nucleonics

TABLE OF CONTENTS

		Page
I.	INTRODUCTION	1
II.	SUMMARY	2
III.	TECHNICAL DISCUSSION	3
	A. MAGNETIC FIELD DIFFUSION INTO THE PROJECTILE AND PROJECTILE HEATING	3
	B. EXPLOSIVE SYSTEM	11
	C. OPTICAL INSTRUMENTATION	16
	D. TEST SHOTS	20
IV.	FUTURE WORK	22
APPENDIX -	MAGNETIC FIELD DIFFUSION AND HEATING COMPUTATION	

LIST OF FIGURES

		Page
1.	Simulated Drive Field for Diffusion and Heating Calculations (applied in outer computation zone)	5
2.	Magnetic Field Diffusion into Aluminum Cylinder, $\eta = a + bT$	7
3.	Magnetic Heating of Aluminum Cylinder, $\eta = a + bT$	8
4.	Magnetic Field Diffusion into Aluminum Cylinder, $\eta = a + \frac{b}{33} T$	9
5.	Magnetic Heating of Aluminum Cylinder, $\eta = a + \frac{b}{33} T$	10
6.	Magnetic Field Diffusion into Aluminum Cylinder, $\eta = \frac{a + bT}{1 + 32B}$	12
7.	Magnetic Heating of Aluminum Cylinder, $\eta = \frac{a + bT}{1 + 32B}$	13
8.	Magnetic Field Diffusion into Aluminum Cylinder, $\eta = \frac{a + bT}{1 + 32B^2}$	14
9.	Magnetic Heating of Aluminum Cylinder, $\eta = \frac{a + bT}{1 + 32B^2}$	15
10.	Multiple Detonator Firing System--Slave Unit	17
11.	Schematic Diagram of Multiple Detonator Firing System	18
12.	Optical System for Direct Viewing of Projectile During Flux Compression	19

I. INTRODUCTION

The objective of this program is to determine the feasibility of using strong magnetic field gradients to accelerate small, metallic projectiles to velocities suitable for simulating micrometeoroid impacts. The gradients are in the megagauss per millimeter range and are obtained by compressing an initial magnetic field with an explosively collapsed metal cylinder.

This quarterly report covers the period from 1 July 1965 through 30 September 1965.

II. SUMMARY

13129

A qualitative analysis was made of magnetic field diffusion into the projectile surface, and projectile heating. Non-linear calculations were performed. Included were computations using empirical functions of resistivity which account for the observed high field anomaly. The results indicate that flux diffisuion and heating should not be a problem.

The transfer of experimental work to the AGN Pulse Power Facility has been completed. There have been some delays caused by electronic failures and explosive procurement problems. A permanent detonator firing slave unit has been built which fires the 24 SE-1 detonator with an average deviation of ± 0.01 μsec.

Optical instrumentation has been developed for directly viewing the projectile during flux compression. Several tests have been conducted to check magnetic gradient accelerator (MGA) subsystem operation. All the basic components for the remainder of the experimental program have been fabricated.

Several projectile experiments have been assembled and await delivery of explosives.

III. TECHNICAL DISCUSSION

A. MAGNETIC FIELD DIFFUSION INTO THE PROJECTILE AND PROJECTILE HEATING

1. Description of Problem

Since the risetime of the magnetic field occurs on a microsecond time scale, there will be partial penetration of the field and its associated current into the surfaces of the armature, flux concentrator and projectile. This flux diffusion will cause flux loss and heating of the metal. Because of the small size of the projectile (1.5 mm diameter), heating is of particular concern; thus the calculations given here simulate the projectile geometry. In a general way, however, they indicate the degree of diffusion into other metal surfaces. As related to surfaces whose radius of curvature is larger than 0.75 mm, the results are conservative.

An analysis of this is necessarily complex. Fundamental factors such as specific heat, electrical conductivity, and rate of magnetic field diffusion are dependent on the time history of the field and its peak value. In addition, effects due to extremes of magnetic and electric field strength, and magnetic pressure are not well known. A rigorous calculation is therefore not possible at this time. To provide some basis for evaluation of the problem, however, a non-linear analysis was performed using available handbook values for physical properties. Hydrodynamics were not included.

The analysis was performed on the diffusion of magnetic flux into a cylinder of the same diameter as the sphere, which is 1.5 mm.

This model was sufficiently similar to provide an estimate of projectile vaporization with a somewhat simpler geometric model. The characteristics of the external driving flux were taken from experimental data, and are shown in Fig. 1. The initial magnetic field strength was 40 kgauss. The method of calculation is given in the appendix.

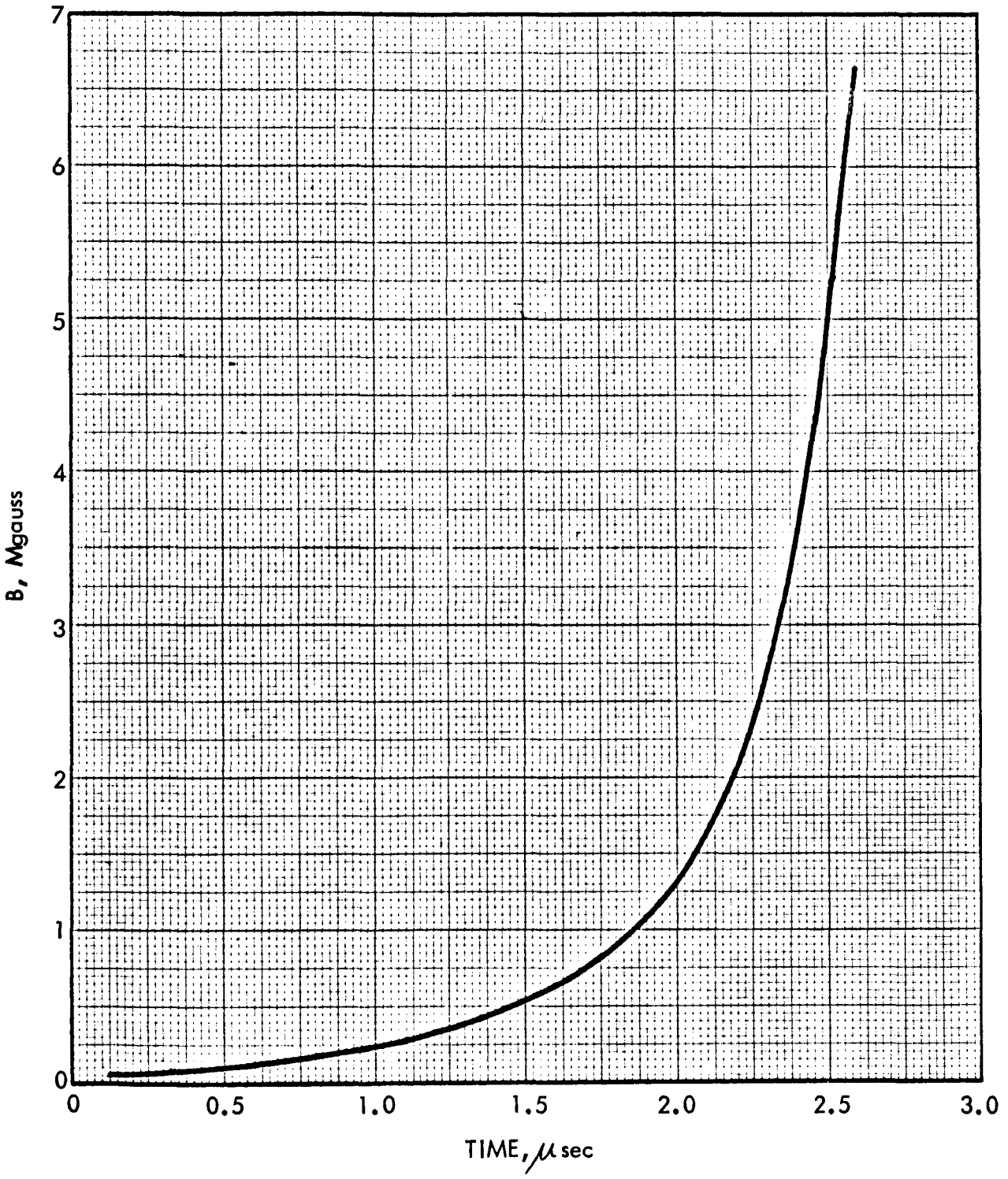

35.1-65-2077

FIGURE 1. SIMULATED DRIVE FIELD FOR DIFFUSION AND HEATING CALCULATIONS (Applied in outer computation zone)

2. Results

Figures 2 and 3 show the radial variation of magnetic flux and temperature for various times for the 1.5-mm cylinder. Vaporization starts to occur in slightly over 2 μsec or about 1.5 Mgauss. The results of the problem after the beginning of vaporization are not better defined than the material properties in that condition.

3. Correction for High Magnetic Field Effects

The calculations described in Section III.A.2 utilized a linear temperature dependence for the resistivity, i.e., $\eta(T) = a + bT$. Subsequent to these calculations AGN was informed of Crawford's experiments, at the Sandia Corporation.[1] These indicated that the temperature coefficient, b, of aluminum, is affected by a strong pulsed magnetic field environment. Although uncertainties were expressed in the results, their measurements showed that b had decreased a factor of 33 at 1 Mgauss.

To test the effect of decreasing b, the magnetic field diffusion and heating calculations were rerun using a fixed correction factor of 33 as an arbitrary average to 5 Mgauss. Thus the resistivity function became $a + (b/33)T$. The resulting diffusion and temperature profiles are shown in Figs. 4 and 5.

No fundamental theory of this phenomenon is known to AGN. It appears, however, that at least magnetic field strength, electric field strength, and pressure are involved. The experimental data available are in terms of magnetic field strength. Empirically, it seemed reasonable that a field dependent resistivity function could vary inversely as B, to a first approximation. The equation used was $\eta(B,T) = a + bT/1 + 32B$ (B in Mgauss) so that it coincided with

[1] J. C. Crawford, Private Communication, Sandia Corporation, Albuquerque, New Mexico.

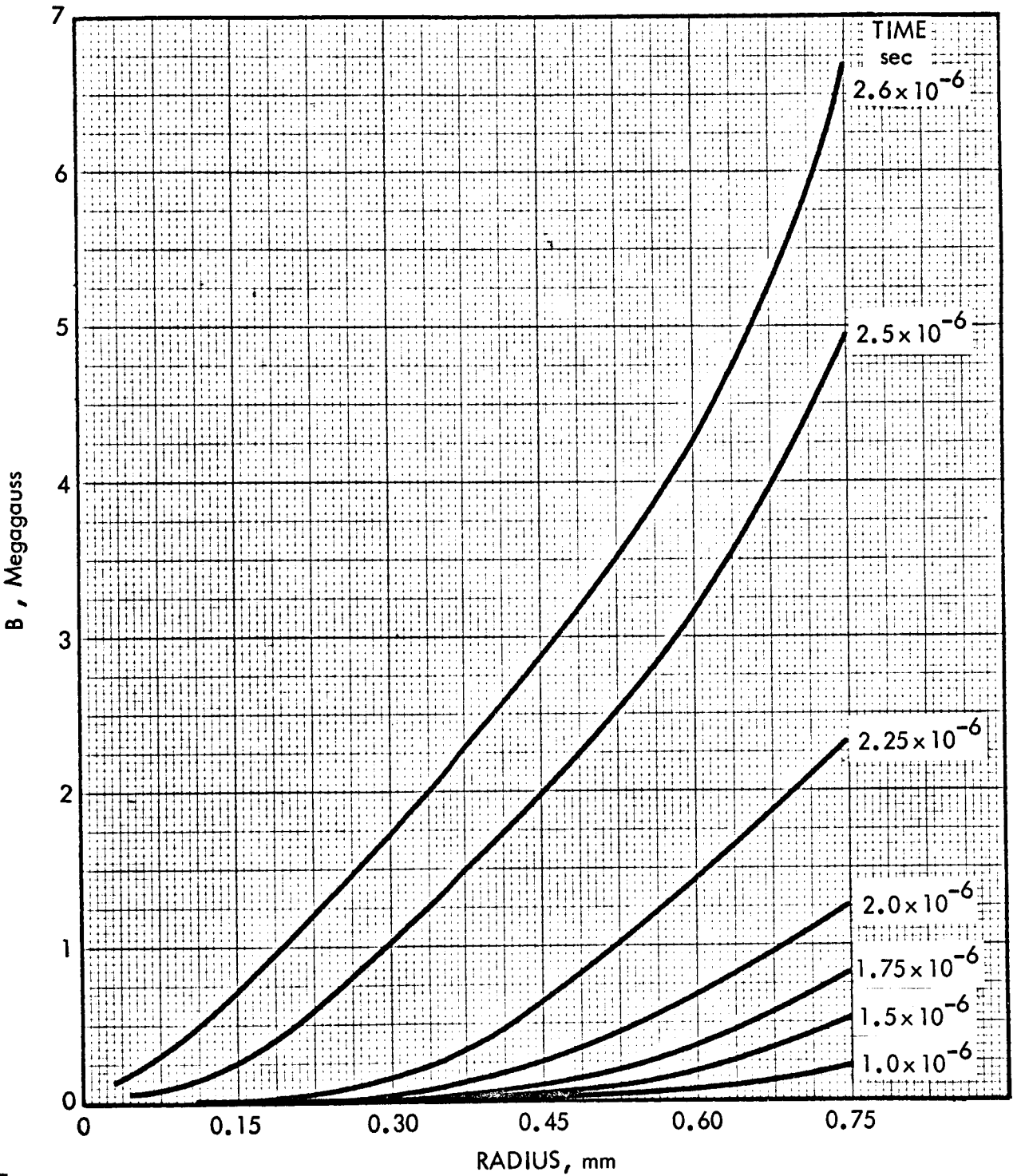

351-65-2066

FIGURE 2. MAGNETIC FIELD DIFFUSION INTO ALUMINUM CYLINDER, $\eta = a + bT$

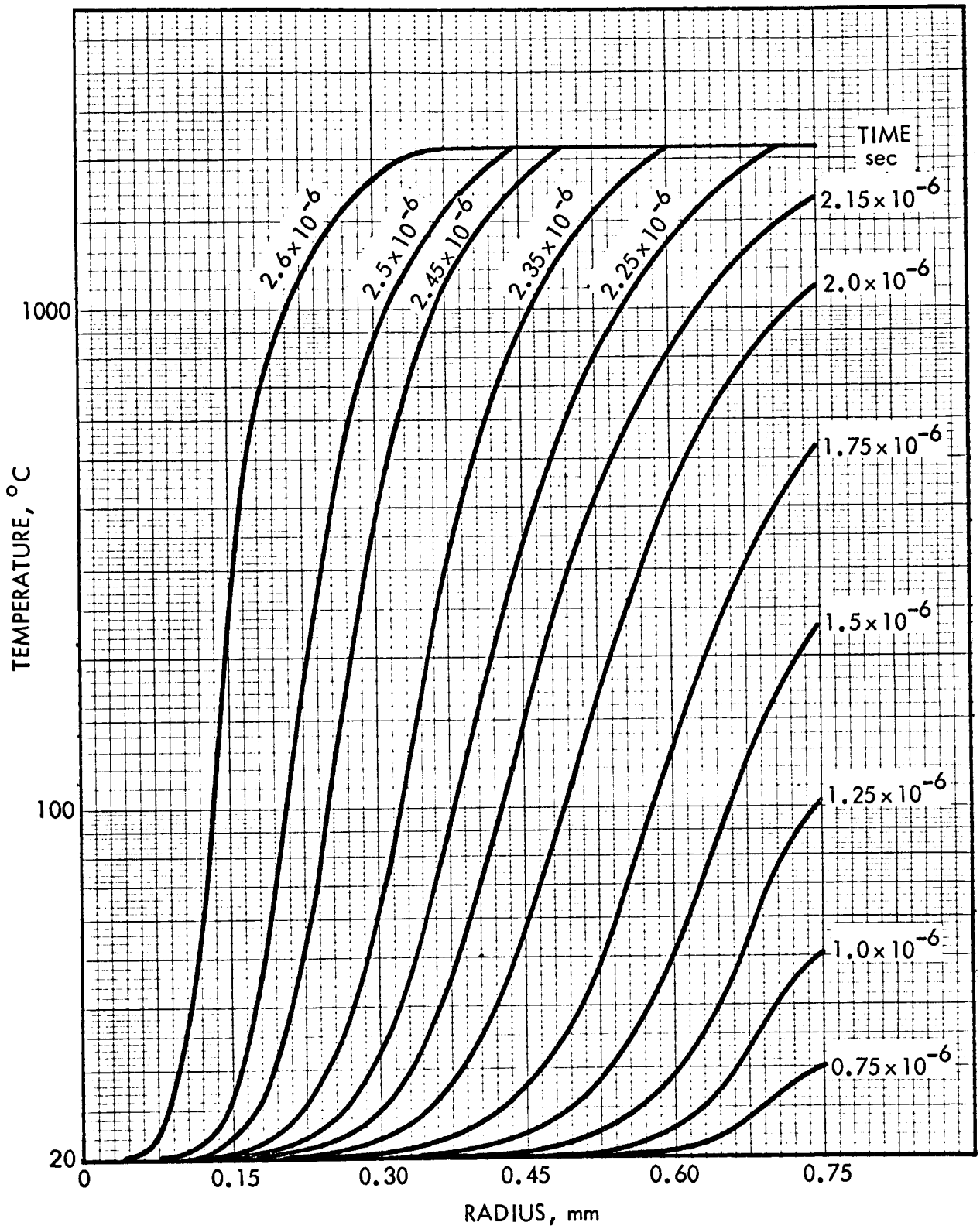

35.1-65-2070

FIGURE 3. MAGNETIC HEATING OF ALUMINUM CYLINDER, $\eta = a + bT$

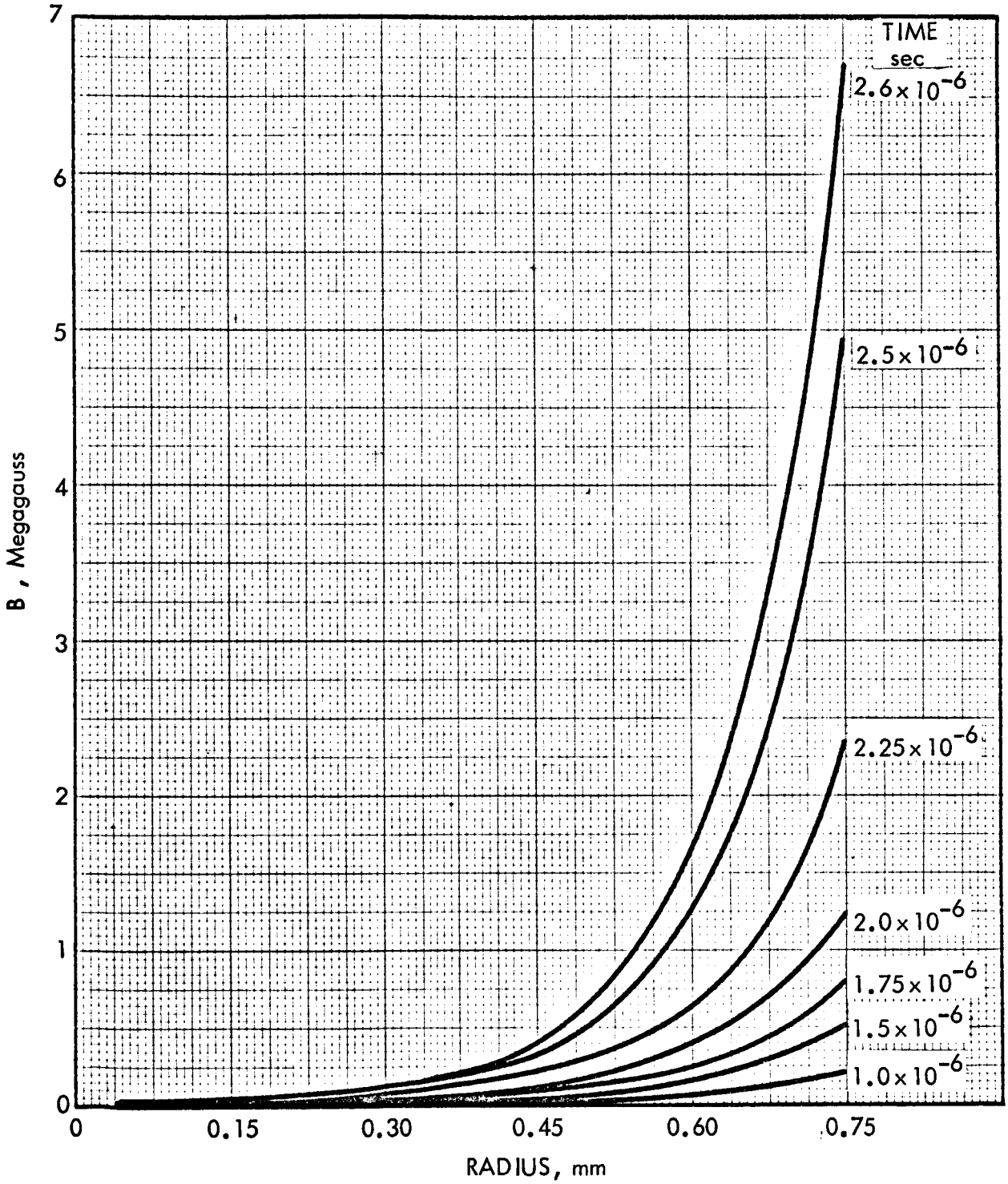

[35.1-65-2067]

FIGURE 4. MAGNETIC FIELD DIFFUSION INTO ALUMINUM CYLINDER, $\eta = a + \frac{b}{33} T$

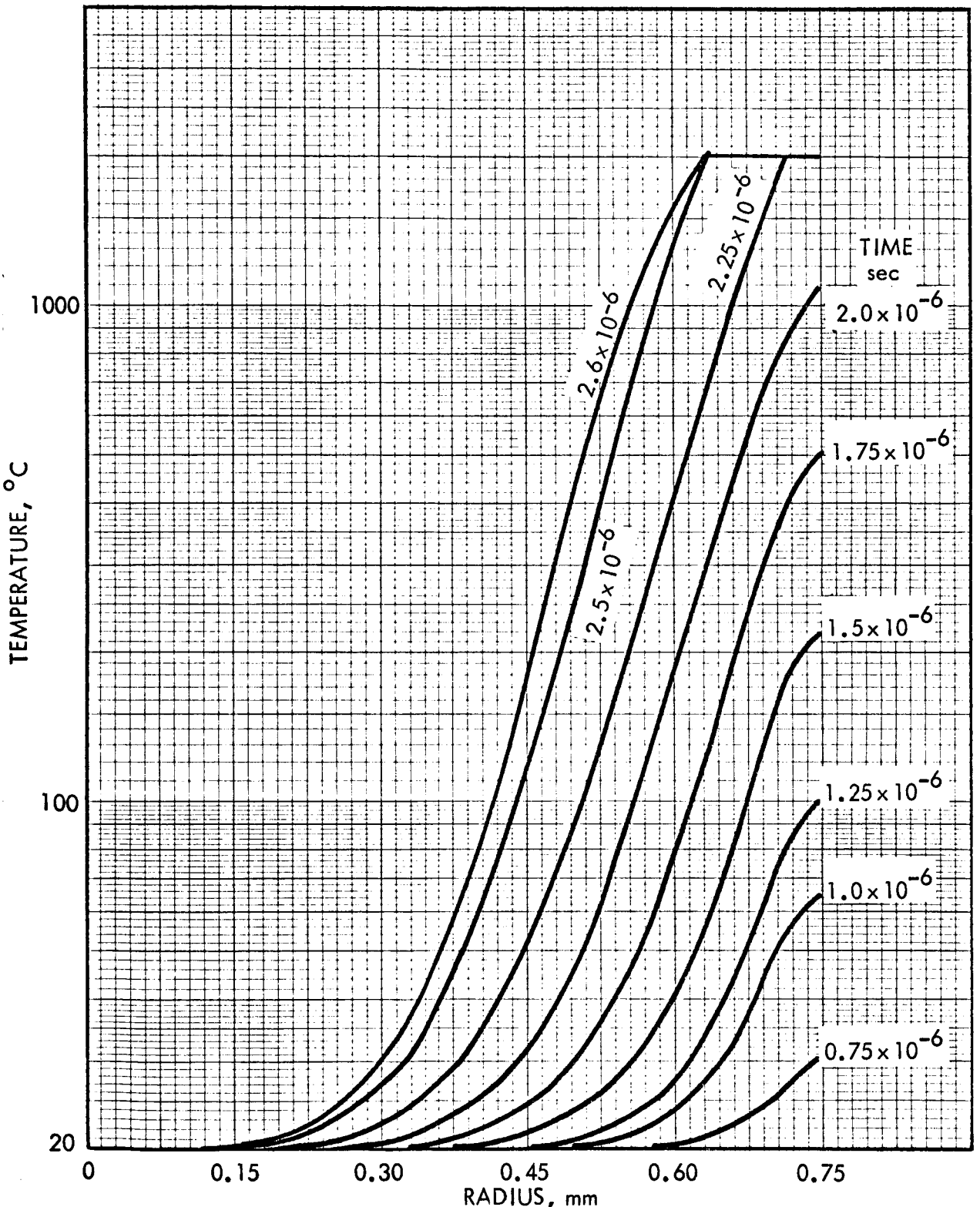

35.1-65-2071

FIGURE 5. MAGNETIC HEATING OF ALUMINUM CYLINDER, $\eta = a + \frac{b}{33} T$

the experimental point. The results are shown in Figs. 6 and 7.

Since static high pressure experiments have shown reduced resistivity, a magnetic field pressure dependence was considered. The effect of this is rather drastic, and probably unrealistic. For purposes of comparison, however, a computation was run using $\eta(B,T) = a + bT/1 + 32\ B^2$, which also matches the experimental point. The results are shown in Figs. 8 and 9.

The results of these calculations follow the expected trend. It is recognized that the functions describing the B dependence of η are crude. Qualitatively, however, it is apparent that this phenomenon causes order-of-magnitude reductions of the magnetic field penetration and heating of small aluminum conductors. Crawford's experiments also indicated an increase of specific heat with B. No attempt was made to include this, thus causing the results to be more pessimistic than they would be otherwise.

B. EXPLOSIVE SYSTEM

At the beginning of this report period the subcontract with Stanford Research Institute was completed and all explosive testing was moved to the AGN Pulse Power Facility. Although operations for this program are much more efficient in our own facility, some delays have been experienced in making the transfer. The explosive cylinders for the main charge were ordered early in the program and quantities of the explosive will be received shortly. Up to now, only three cylinders have been delivered.

As a backup measure, a quotation has been requested and received from the AEC Pantex Plant operated by the Mason and Hanger Company at Amarillo, Texas. Fabricated explosive has been ordered from them but the time required for the necessary approvals and fabrication will place first delivery quite late in this program.

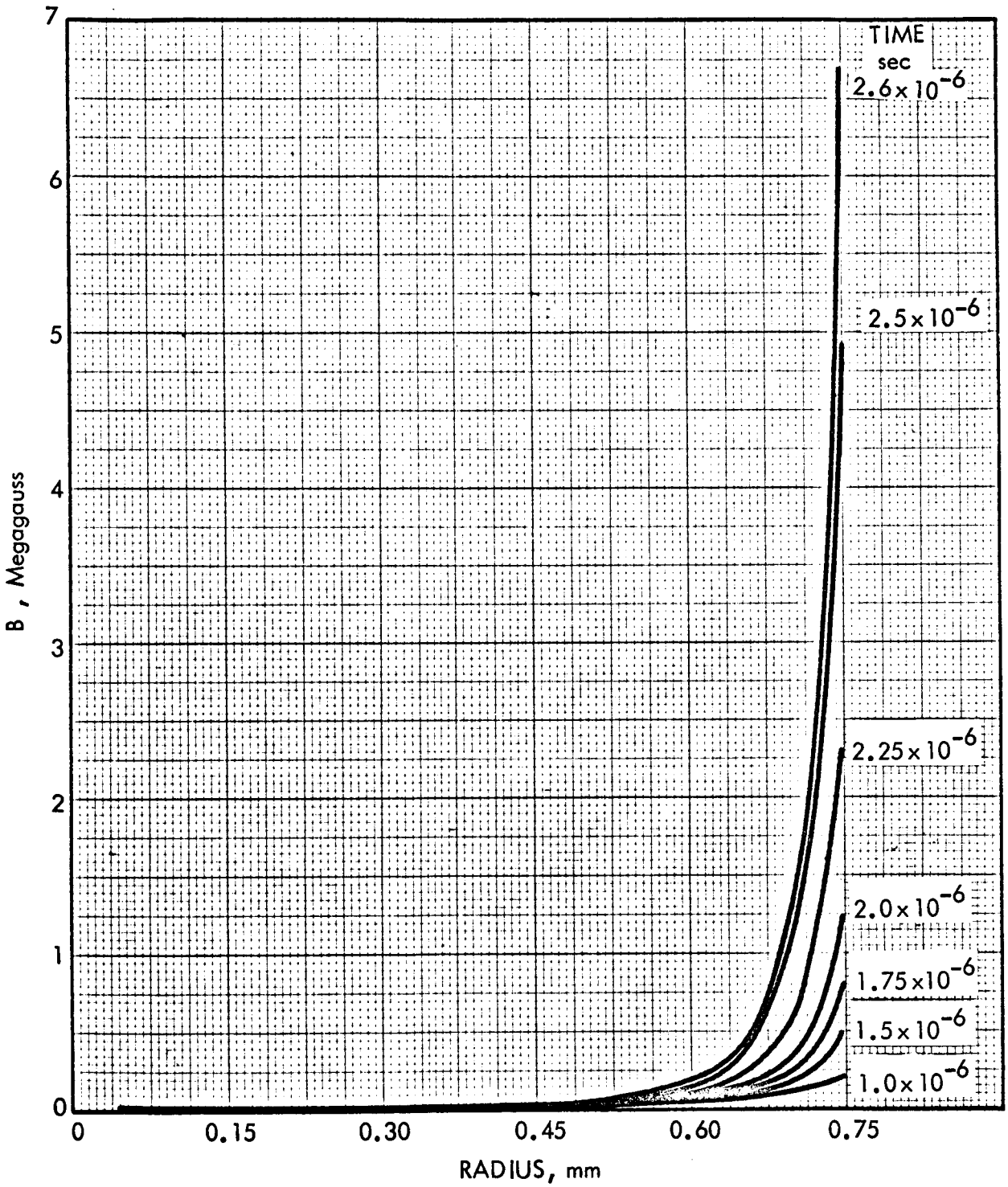

35.1-65-2068

FIGURE 6. MAGNETIC FIELD DIFFUSION INTO ALUMINUM CYLINDER, $\eta = \frac{a+bT}{1+32B}$

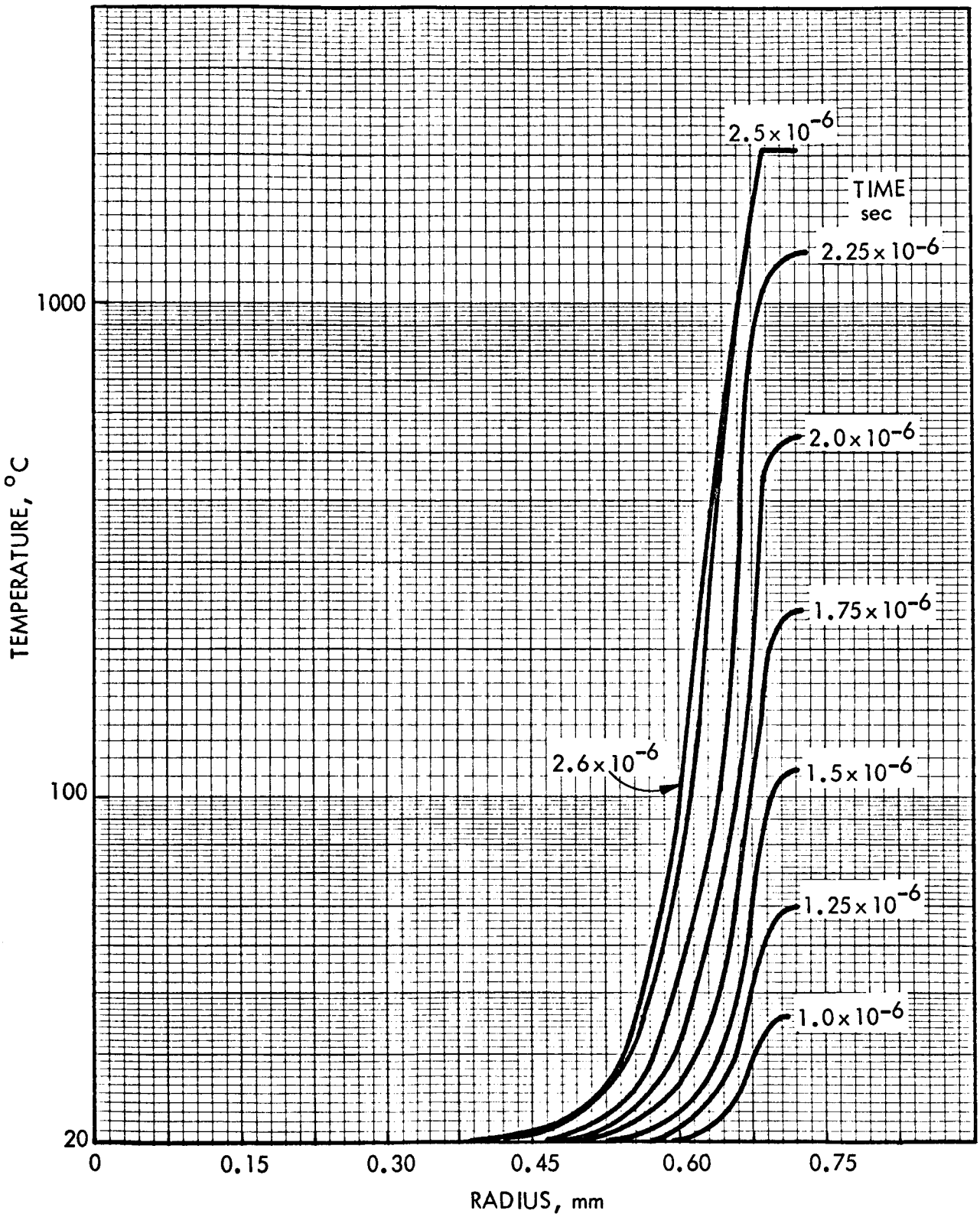

351-65-2072

FIGURE 7. MAGNETIC HEATING OF ALUMINUM CYLINDER, $\eta = \frac{a+bT}{1+32B}$

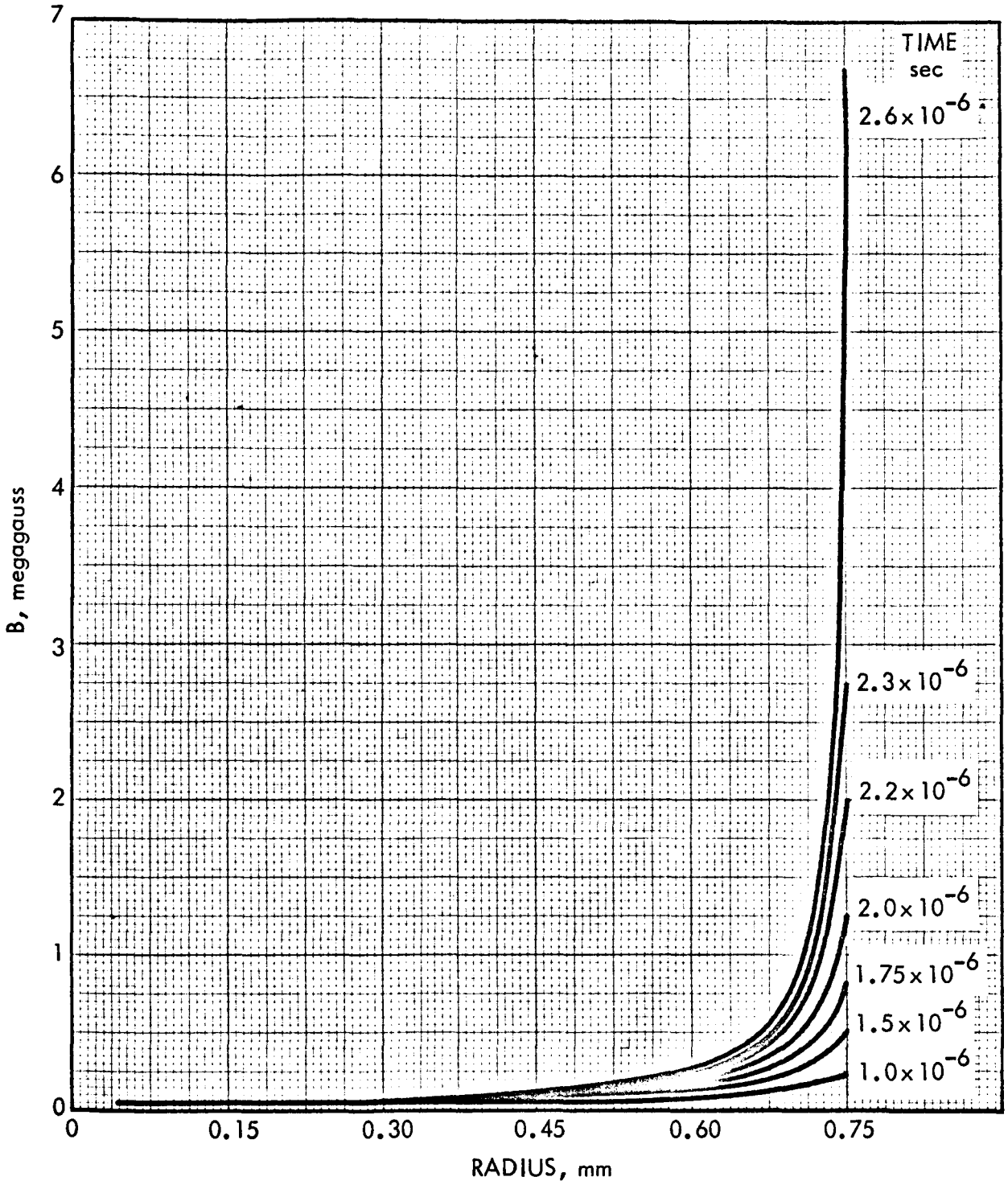

35,1-65-2064

FIGURE 8. MAGNETIC FIELD DIFFUSION INTO ALUMINUM CYLINDER, $\eta = \frac{a+bT}{1+32\,B^2}$

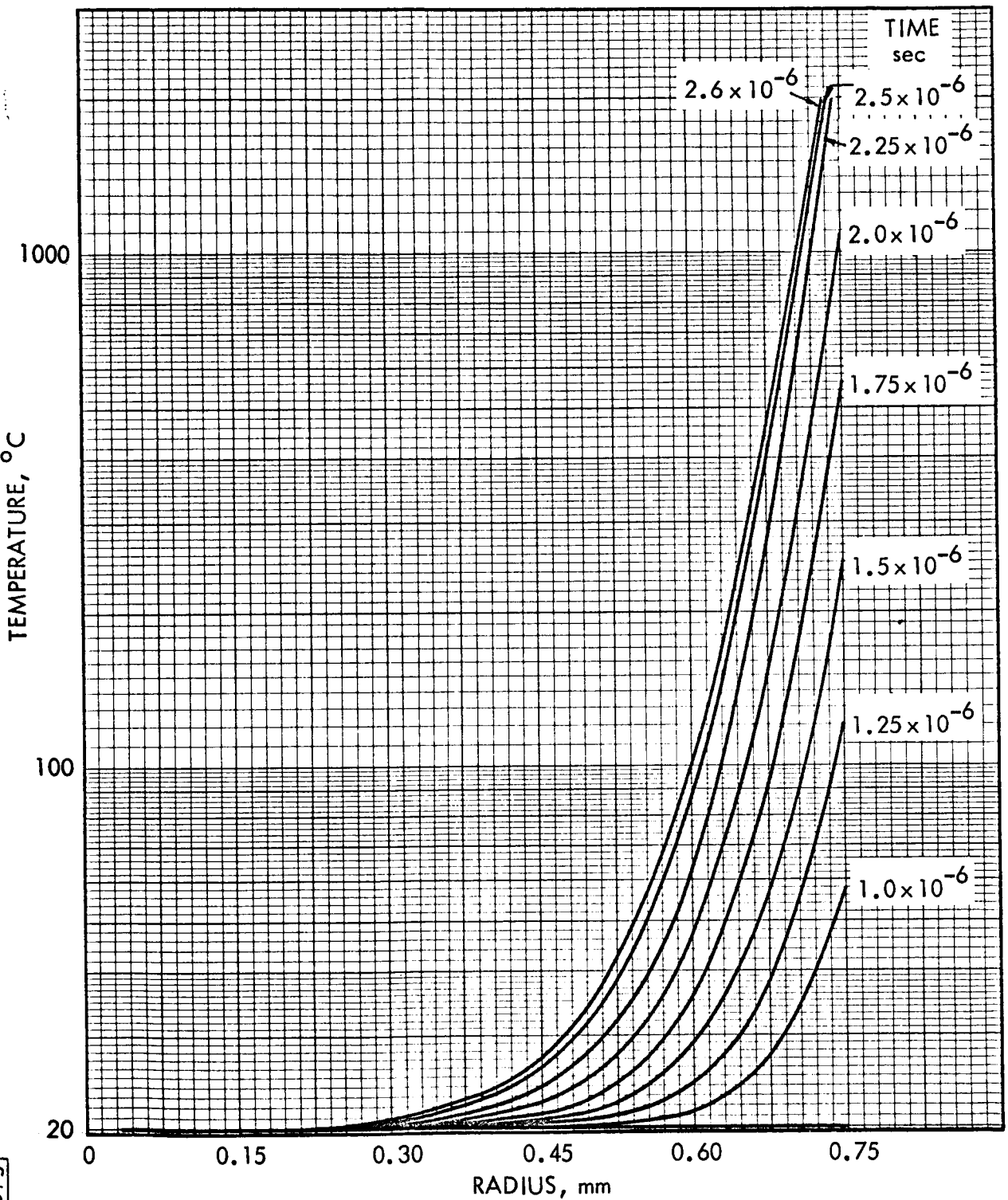

351-65-2073

FIGURE 9. MAGNETIC HEATING OF ALUMINUM CYLINDER, $\eta = \frac{a+bT}{1+32B^2}$

During the transfer period from SRI to AGN, it was realized that a non-expendable detonator firing system of much better design would be not only desirable but necessary for both precision and economical operation. Also, it was necessary to modify the primary detonator firing panels in the AGN Pulse Power Facility so that they would operate with a slave discharge system. The slave unit which was built for this purpose is illustrated in Fig. 10. It is located just outside the explosion containment tank and is completely reusable. Its special low inductance design produces an extremely fast discharge pulse necessary for simultaneous firing of the 24 SE-1 detonators. A simplified schematic circuit diagram of the complete detonator firing system is shown in Fig. 11. This system will fire all 24 detonators with an average deviation of ± 0.01 μsec.

The main firing and control system in the pulse power facility also contributed somewhat to delay in the experimental work. A series of component failures, necessitating procurement of special parts for replacement, delayed required testing of the initial explosive charges. Functioning of the detonator system has been quite satisfactory since about the third week of August, however.

C. OPTICAL INSTRUMENTATION

It has been necessary to devise a special optical system for direct viewing of the projectile during the flux compression. This requires high magnification so that the 1.5 mm diameter projectile will virtually fill the frame of the framing camera. Certain restrictions are imposed by the optical characteristics of the camera itself and its objective lens. The arrangement illustrated in Fig. 12, however, appears to be quite satisfactory. The first objective lens in Fig. 12

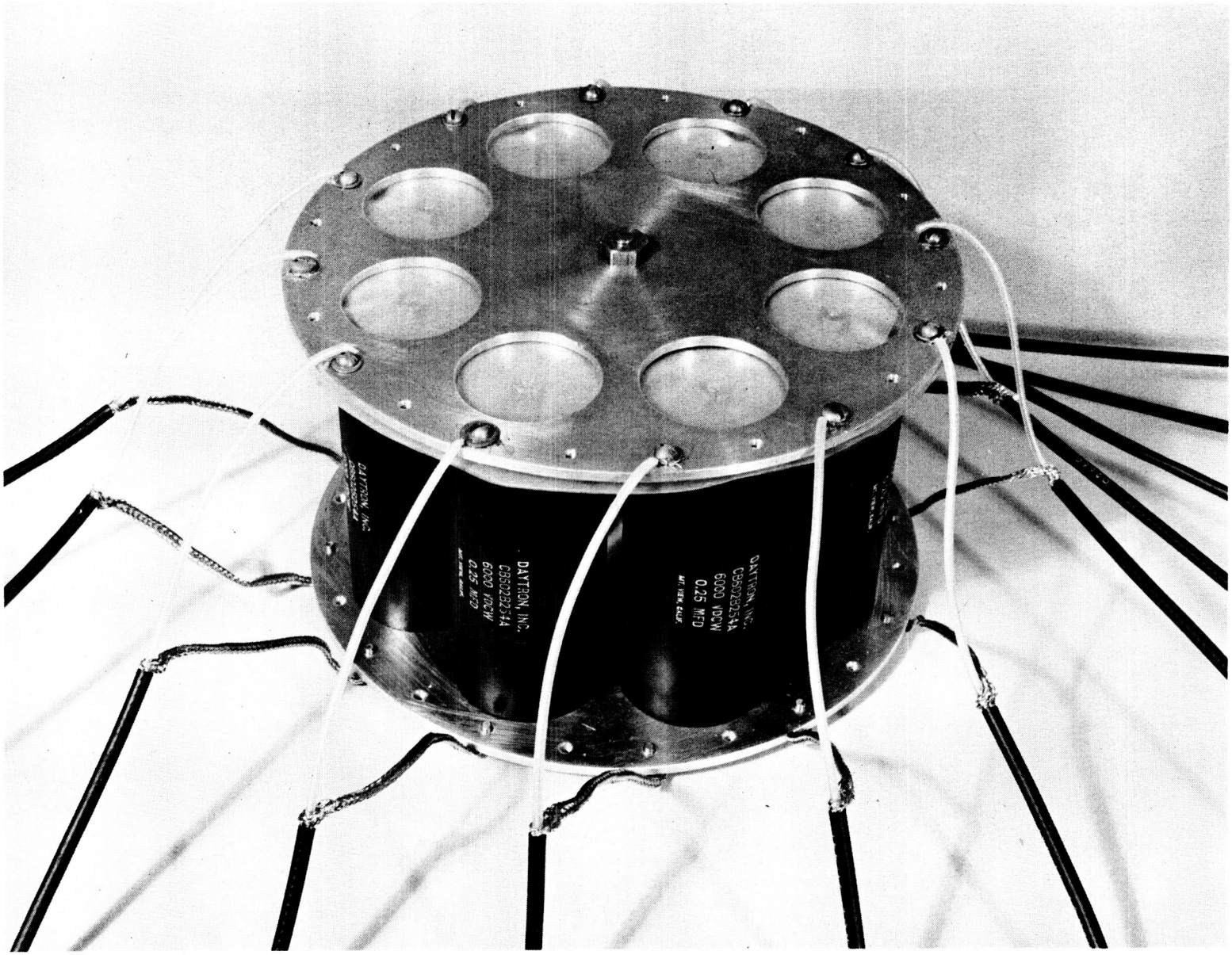

FIGURE 10. MULTIPLE DETONATOR FIRING SYSTEM - SLAVE UNIT

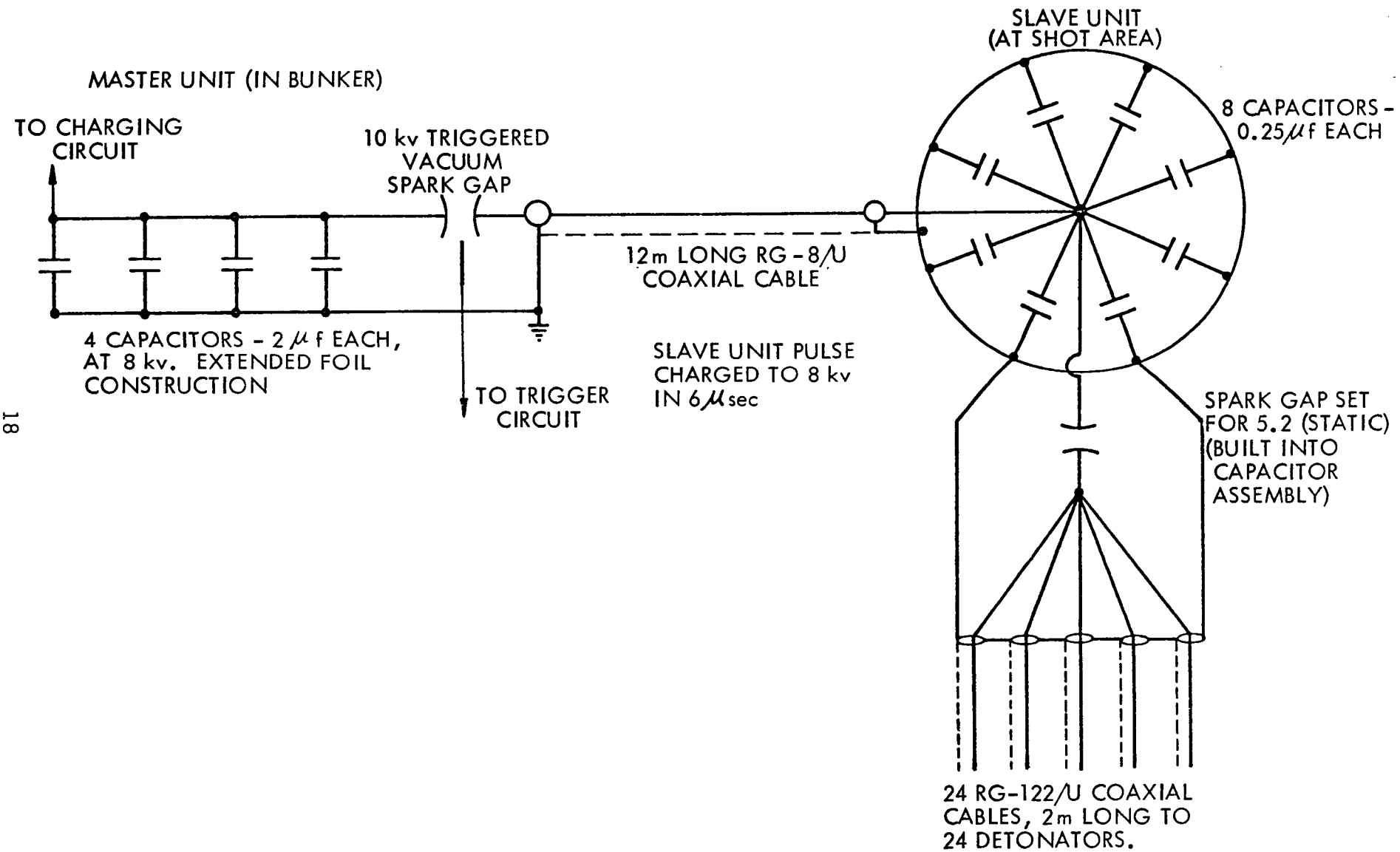

FIGURE 11. SCHEMATIC DIAGRAM OF MULTIPLE DETONATOR FIRING SYSTEM

87.1-65-2248

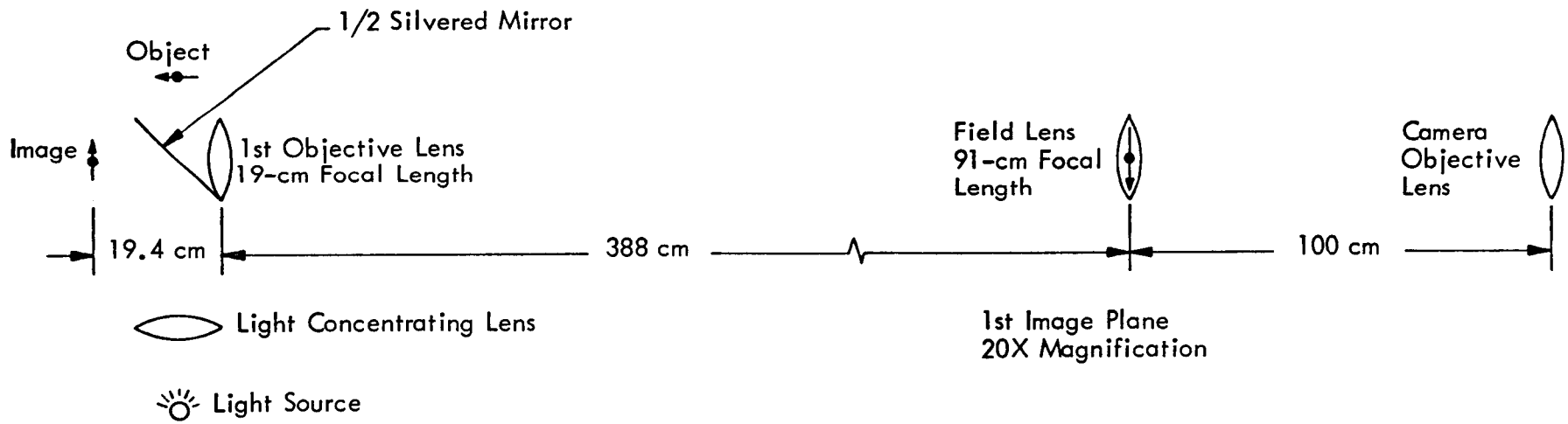

FIGURE 12. OPTICAL SYSTEM FOR DIRECT VIEWING OF PROJECTILE DURING FLUX COMPRESSION

provides the magnification which is about X20. The field lens placed at the image point formed by the first objective lens redirects the light rays from the aerial image, thus making the image seen by the camera considerably brighter.

One problem which as yet does not have a satisfactory solution is the illumination of the projectile. An extremely intense light source is required. It will be concentrated by a lens onto the projectile as shown in Fig. 12. The half-silvered mirror which must be used causes a light loss of a factor of 4.

Previous attempts at illuminating the projectile using an intense xenon flash lamp have proven inadequate. The next method to be tried will be the use of an exploding bridge wire. If this does not work it may be necessary to design a special explosive argon candle with some sort of light piping or mirror system to direct the light rays up into the flux concentrator throat.

D. TEST SHOTS

Several subsystem test shots have been fired to check out the multiple detonator firing system and the fiber optics streak camera hydrodynamic instrumentation technique. Also, three tests using the full explosive system were fired. One of these was a magnetic compression shot. The purpose of these tests was to check out fundamental operations and techniques in the AGN Pulse Power Facility, and to test the precision of the explosive system. Since tests of this type have been conducted before in this program they will not be described in detail. In general, however, the results are quite satisfactory. In particular, the detonator firing system produced an average deviation of ± 0.01 μsec over the 24 detonators. This is 3 to 4 times better than has been previously achieved. The three main explosive charges which have been obtained have produced adequate

performance but could be improved. Some changes have been made in the fabrication technique at Aerojet's Ordnance Facility to correct some of the discrepancies which occurred in the first manufacturing run.

During this report period, basic components have been fabricated for all tests to be conducted. These include the magnet coils, explosive tamping plates, armatures, and shock absorbing pads. Other operational preparations have also been made so that shots can be fired at a relatively high rate. Also, several experiments have been prepared and at the present time are awaiting delivery of explosives.

IV. FUTURE WORK

All future work will be experimental and concerned with projectile acceleration. The evacuated armature shot will test for the source of the luminous, high velocity cloud of gas which has been observed in previous experiments. The up-the-throat optics shots will examine the projectile during the flux compression. Also, there is a possibility that the projectile is being trapped by the armature. This will be investigated. Once the explosives are received the experimental work should progress at a rapid rate.

APPENDIX

MAGNETIC FIELD DIFFUSION AND HEATING COMPUTATION

An axial magnetic flux is initially uniformly distributed both internally and externally to an infinitely long aluminum cylinder 1.5 mm in diameter. The concentric volume surrounding the cylinder is rapidly compressed so that the flux external to the cylinder increases without loss. The magnetic field strength-time history is taken from experimental measurements.

The physical boundary conditions at the surface require that the axial magnetic field be the same internal and external to the surface. As the axial magnetic flux diffuses into the metal, an electric current is induced in the circumferential direction which causes heating of the material. The heat deposition has the same radial distribution as the current generating it, but the time of the transient is so short that there can be no appreciable diffusion. Thus the temperature increases only in the local area where the heat deposition occurs.*

The material properties which affect the distribution and diffusion are the magnetic permeability μ, the specific heat c_p, and the resistivity η. The material is non-magnetic, has a permeability equivalent to a vacuum and is considered to be a constant in these problems. The specific heat and resistivity are both functions of temperature and thus have a spatial distribution associated with the temperature distribution.

*Typical heat deposition occurs at 10^4 times the rate of removal by thermal diffusion.

The requirements of the calculation are the determination of the spatial and time dependent current and temperature distribution. The electrodynamic character of the cylinder can be described by Maxwell's equations,

$$\nabla \cdot \bar{D} = \rho = 0 \tag{1}$$

$$\nabla \cdot \bar{B} = 0 \tag{2}$$

$$\nabla \times \bar{E} = -\frac{\partial \bar{B}}{\partial t} \tag{3}$$

$$\nabla \times \bar{H} = \bar{J} + \frac{\partial \bar{D}}{\partial t} = \bar{J} \tag{4}$$

Ohms law,

$$\bar{E} = \eta \bar{J} \tag{5}$$

and the permeability equation,

$$\bar{B} = \mu \bar{H} \tag{6}$$

The thermal characteristics of the load are expressed by

$$\rho c_p \frac{\partial T}{\partial t} = \nabla \cdot (k \nabla T) + \eta J^2 \tag{7}$$

The first problem is to evolve an expression for the spatial and time dependent distribution of the magnetic field vector $\bar{H}$. This is accomplished by taking the curl of Eq. (4) and then successively substituting in Eqs. (5), (6) and (7), and expanding as follows:

$$\nabla \times \nabla \times \bar{H} = \nabla \times \bar{J} = \nabla \times \left(\frac{1}{\eta} \bar{E}\right)$$

$$\nabla (\nabla \cdot \bar{H}) - \nabla^2 \bar{H} = \nabla \left(\frac{1}{\eta}\right) \times \bar{E} + \left(\frac{1}{\eta}\right) \nabla \times \bar{E}$$

$$\nabla (\nabla \cdot \bar{H}) - \nabla^2 \bar{H} = \nabla \left(\frac{1}{\eta}\right) \times (\eta [\nabla \times \bar{H}]) - \frac{\mu}{\eta} \frac{\partial \bar{H}}{\partial t}$$

Now the magnetic field vector has only one component, $\bar{H}_z(r)$, and the scalar resistivity is also a function, $\eta(r)$, varying only in the radial direction. Inserting these components we find that

$$\nabla \cdot \bar{H} = 0 \quad \text{and} \quad \nabla(\nabla \cdot \bar{H}) = 0$$

$$\nabla^2 \bar{H} = \bar{z}\left[\frac{1}{r}\frac{\partial}{\partial r}\left(r\frac{\partial H_z(r)}{\partial r}\right)\right]$$

$$\nabla\left(\frac{1}{\eta}\right) \alpha \left(\eta[\nabla \times \bar{H}]\right) = \bar{z}\left[\left(\frac{\partial\left(\frac{1}{\eta(r)}\right)}{\partial r}\right)\eta(r)\left(-\frac{\partial H_z(r)}{\partial r}\right)\right]$$

$$\frac{\mu}{\eta}\frac{\partial \bar{H}}{\partial t} = \bar{z}\left[\frac{\mu}{\eta(r)}\left(\frac{\partial H_z(r)}{\partial r}\right)\right]$$

where $\bar{z}$ is the unit vector in the z direction. Since the vector components are all in the same direction, the following scalar equation can be formed wherein $H_z(r)$ is written as $H(r)$.

$$\frac{\partial H(r)}{\partial t} = \frac{\eta(r)}{\mu}\left[\frac{1}{r}\frac{\partial}{\partial r}\left(r\frac{\partial H(r)}{\partial r}\right) - \eta(r)\left(\frac{\partial\left(\frac{1}{\eta(r)}\right)}{\partial r}\right)\left(\frac{\partial H(r)}{\partial r}\right)\right] \quad (8)$$

The boundary conditions on the equation are that the radial gradient of H(0) equal zero and that H(r) is equal to a known, time-varying, magnetic field vector, Equation (8) can be rewritten, expanding the spatial distribution in a finite difference form for K + 1 equally thick radial segments, i.e., $0 \leq k \leq K$.

$$\frac{\partial H(r)}{\partial t}\Big|_k = \frac{\eta k}{\mu}\left\{\frac{1}{r_k}\left[\left(\frac{2r_k + \Delta r}{2\Delta r^2}\right)\left(H_{k+1} - H_k\right)\right.\right.$$

$$\left. + \left(\frac{2r_k - \Delta r}{2\Delta r^2}\right)\left(H_{k-1} - H_k\right)\right]$$

$$\left. - \eta_k\left(\frac{H_{k+1} - H_{k-1}}{2\Delta r}\right)\left(\frac{\left(\frac{1}{\eta}\right)_{k+1} - \left(\frac{1}{\eta}\right)_{k-1}}{2\Delta r}\right)\right\} \quad 1 \leq k < K \qquad (9a)$$

$$H_o = H_1 \qquad (9b)$$

$$H_k = f(t) \qquad (9c)$$

where f(t) is the known time variation of the magnetic field vector external to the cylinder.

The equations describing the temperature distribution are obtained by writing Eq. (7) in a finite difference form. The transient process is quite fast, on the order of 2.5 μ sec, so that thermal diffusion has a very limited effect, i.e., $\nabla \cdot (k \nabla T) << J^2$ and Eq. (7) can be written as

$$\rho c_p \frac{\partial T}{\partial t} = \eta J^2$$

or in finite difference form as

$$\frac{dT}{dt}\Big|_k = \left(\frac{1}{\rho c_p}\right)_k (\eta i)_k i_k o \quad k = 0,1,2, \ldots K \qquad (10)$$

In this equation, c_p is a function of the temperature of the zone. The current can be evaluated directly from Eq. (4) by noting that the currents are limited to the circumferential direction and are only a function of radius so that Eq. (4) can be expanded to

$$i(r) = \frac{\partial H(r)}{\partial r} \tag{11}$$

or in finite difference form

$$i_k = \frac{H_{k+1} - H_{k-1}}{2\,\Delta r} \qquad 1 \leq k < K \tag{12a}$$

$$i_k = \frac{H_k - H_{k-1}}{\Delta r} \tag{12b}$$

$$i_o = 0$$

In summary, the vector equations have been reduced to a set of ordinary, non-linear, first-order, coupled, differential equations in the single independent variable, time, and a number of algebraic equations which are used to determine the nodal currents. This set of equations is compatible, and can be solved using an integrating scheme such as the Adams routing. A digital computer code, MIMIC,[2] was used to solve these equations using an IBM 7094. The code is designed to provide a solution to a general set of equations of the type encountered in this problem, using a high order Runge-Kutta integration method. The time step is determined based on error criteria for the dependent variables.

A set of problems was run using a 1.5-mm diameter aluminum rod. These computations used 20 equal radial increments and temperature dependent specific heat and resistivity properties. These properties were approximated by the following linear equations

$$\eta(T) = 2.824 \times 10^{-8} \times 0.011 \times 10^{-8}\, T \tag{13}$$

$$\frac{1}{\rho\, c_p}(T) = 0.33 \times 10^{-6} - 1.0 \times 10^{-10}\, T \tag{14}$$

---

[2] H. E. Peterson and F. J. Sansom, MIMIC-A Digital Simulator Program, SESCA Internal Memo 65-12, May 1965.

The driving magnetic flux was a simulation of experimental data. It consisted of an exponentiation at the rate of $1.72 \times 10^{+6}$/sec during the first 2.1×10^{-6} sec and then at $3.0 \times 10^{+6}$/sec until the problem was terminated. Initial magnetic field strength of 4×10^{4} gauss was used.

The problems were run so that the temperature of the node would be clamped when that node reached its vaporization temperature ($2057^{\circ}C$). Heat generation was allowed to continue until vaporization had occurred to some extent.